Journal of Zhejiang University-SCIENCE A 2025 26(11):1021-1033
www.jzus.zju.edu.cn; www.springer.com/journal/11582
E-mail: jzus_a@zju.edu.cn

Research Article
https://doi.org/10.1631/jzus.A2400484

Reliability-based optimization of laterally loaded piles with necking defects

Yang YU[1,2], Bo SHI[1], Qing LÜ[3]✉, Chaofeng WU[1,4]

[1]*Ocean College, Zhejiang University, Zhoushan 316021, China*
[2]*Hainan Institute of Zhejiang University, Sanya 572025, China*
[3]*College of Civil Engineering and Architecture, Zhejiang University, Hangzhou 310058, China*
[4]*China Energy Engineering Group Zhejiang Electric Power Design Institute Co., Ltd., Hangzhou 310012, China*

Abstract: Laterally loaded piles, which are commonly used in sandy stratum foundations, are particularly susceptible to necking defects during cast-in-place installation due to borehole collapse risks. These construction-induced geometric imperfections substantially compromise pile safety under lateral loading conditions. To address this critical design challenge, we develop a reliability-based multi-objective optimization framework that simultaneously accounts for structural safety, construction economy, and design robustness. The proposed methodology integrates the *p*-*y* curve (where *p* is the soil pressure per unit length, and *y* is the lateral deflection of the pile) analysis with stochastic modeling, enabling efficient evaluation of pile performance considering uncertainties in soil parameters and depth and size variations of necking defects. A systematic design framework is implemented and validated through experimental case studies, successfully generating optimal designs along the Pareto front. The identified knee-point configurations serve as practical compromise solutions for engineering decisions. Parametric investigations further elucidate the influence of necking defect depth and sand friction angle variations on optimal design outcomes, offering insights into risk mitigation for pile construction.

Key words: Necking defect; Laterally loaded pile; Soil parameter uncertainties; Foundation construction design; *p*-*y* curve analysis; Stochastic modeling

1 Introduction

Laterally loaded piles are common elements of foundations in sandy strata (Sun et al., 2023; Zhou et al., 2024). In the course of cast-in-place pile installation, borehole wall instability during drilling frequently induces localized collapse, creating necking defects. These defects reduce the lateral load capacity by decreasing the cross-sectional area, making it vital for infrastructure safety to accurately predict their spatial distribution and severity. However, variations in the mechanical properties of sand create significant uncertainties in defect characteristics, making the accurate pre-construction prediction of defects difficult. Current practice involves post-installation defect identification and subsequent impact quantification, a process that delays projects and increases costs. This highlights the need for design-phase mitigation strategies that can control deformations and enhance the safety of cast-in-place piles.

The influence of necking defects on foundation pile responses has been investigated by various researchers. For instance, Xu and Poulos (2000) studied the impact of necking defects on pile stiffness, employing both experimental and theoretical analyses of model piles. Poulos (2005) investigated the relationship between defect severity and stiffness reduction using load-settlement curves. The results indicated that the stiffness reduction is more pronounced when the defect is located at or near the surface, rather than at depth. Li et al. (2018) investigated the response of laterally loaded piles in different soils based on the constructed *p*-*y* curve (where *p* is the soil pressure per unit length, and *y* is the lateral deflection of the pile). The applicability of the *p*-*y* curve to laterally loaded piles has been validated using data from both a 1*g* (*g* is the acceleration due to gravity) model experiment

✉ Qing LÜ, lvqing@zju.edu.cn
Yang YU, https://orcid.org/0000-0001-8021-4401

Received Oct. 21, 2024; Revision accepted May 1, 2025;
Crosschecked Sept. 29, 2025; Online first Nov. 10, 2025

and a field experiment. Xu and Guo (2021) conducted experiments to ascertain the influence of necking defects on the bearing capacity of vertically loaded piles. Their findings indicated that the pile's bearing capacity declined more markedly when the necking defect was situated closer to the pile's upper extremity, and when the necking defect was situated in the same location, the bearing capacity of the pile decreased even more significantly as the diameter of the necking defect was reduced. Furthermore, researchers have investigated the impact of necking defects on the performance of laterally loaded piles. Fattah et al. (2010) employed the finite element method to examine the behavior of laterally loaded piles in sand. Their results demonstrated that the deflection of the pile diminished with an increase in the depth of the necking defect (relative to the ground surface). Hariswaran and Premalatha (2021) discovered that necking defects reduced the ultimate bearing capacity of laterally loaded piles in a 1*g* model experiment, particularly when the necking defect was situated near the ground surface.

To assess the impact of necking defects on the performance of pile foundations, it is essential to identify such defects in practical settings. With this in mind, Lee et al. (2018) employed electromagnetic waves to identify necking defects in bored piles. While this method can enhance detection efficacy, the negative impacts of necking defects must ultimately be addressed through replacement or repair of the affected pile. This approach will result in increased costs of labor, materials, and time. Therefore, if necking defects can be reduced or prevented during the design phase, these aforementioned costs could be decreased. However, the inherent uncertainties in soil parameters present a significant challenge in pile design (Yu et al., 2024). To address these challenges, the reliability-based design (RBD) method is frequently employed. As demonstrated by Stuedlein et al. (2012), the RBD represents an effective methodology for addressing the uncertainties associated with soil parameters in pile foundation design. Li et al. (2015) leveraged reliability theory in conjunction with test data collected from Shanghai, China, and accordingly modified the local design code for pile foundations. Moreover, Schmoor and Achmus (2020) evaluated sand pile performance using optimized design parameters through the RBD method. However, in these studies, only the uncertainties in soil parameters were considered. Because necking defects can impact the design parameters of a pile (e.g., diameter), it is essential to comprehensively consider the uncertainties associated with both soil and design parameters.

As mentioned earlier, the robust geotechnical design (RGD), as proposed by Juang and Wang (2013), may be an effective method for designing piles prone to necking defects. In the RGD framework, the input parameters are classified into two categories: design parameters and noise factors. The objective of RGD is to ensure the robustness of a geotechnical system (e.g., the deformation of a laterally loaded pile) to fluctuations in noise factors (e.g., uncertain soil parameters) while maintaining compliance with safety standards by optimizing the design parameters. Peng et al. (2017) employed Monte Carlo simulation (MCS) to enhance the practical applicability of the RGD method. The application of MCS to rock slope design demonstrated that RGD based on MCS is more intuitive and efficient. Furthermore, the effectiveness of the RGD method in stabilizing pile design has been demonstrated by Wang et al. (2020) and Yu et al. (2020), and its suitability for braced excavations by Khoshnevisan et al. (2017). These studies illustrate RGD's capacity to address uncertainties in both soil and design parameters. Nevertheless, further investigation is required to determine the optimal design of laterally loaded piles using the RGD framework, particularly with regard to potential necking defects. Additionally, the effectiveness of such an approach must be substantiated through practical engineering applications or rigorous testing.

The rest of this study is organized as follows: In Section 2, a methodology for assessing the responses in a laterally loaded pile with necking defects is presented. Section 3 describes a robust design framework for a laterally loaded pile that considers the inherent uncertainties in both soil parameters and necking defects. In Section 4, the proposed method is validated by experimental data. Subsequently, the proposed framework is applied towards the optimal design of a laterally loaded pile with necking defects. The factors affecting the optimal design are discussed in Section 5, and conclusions are given in Section 6.

2 Method for evaluating responses of a laterally loaded pile with necking defects

2.1 Spreadsheet method

Fig. 1 illustrates a conceptual model of a laterally loaded pile exhibiting a necking defect. In this context,

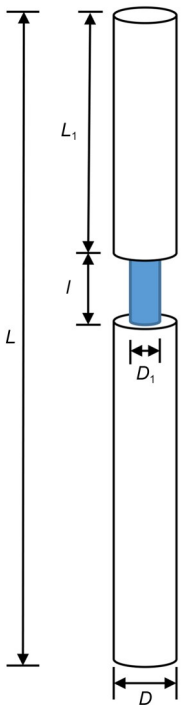

Fig. 1 Schematic of the necking defect of a laterally loaded pile

the symbols L and D represent the length and diameter of the pile, respectively. The necking defect is situated at a depth of L_1 below the pile top. The dimensions of the necking defect are defined by its length l and diameter D_1 (where $D_1<D$). The laterally loaded pile is decomposed into a series of beam elements, and the responses of these elements, including deflection and internal forces, are solved for using the spreadsheet method (Low et al., 2001). Fig. 2 shows a typical spreadsheet for a laterally loaded pile with a necking defect. It includes formulations for calculating bending moment, shear force, and deflection, which will next be introduced in detail.

The coordinates of each node of the beam elements are presented in Cells C7–C23 in Column z_i. The value in each cell is calculated with:

$$z_i=z_{i-1}+r_{\Delta z}(z_{i-1}-z_{i-2}),\quad i>2, \tag{1}$$

where $r_{\Delta z}$ is the common ratio. In the spreadsheet method extruded in Microsoft Excel, the GoalSeek function is used to calculate $r_{\Delta z}$ under the constraint

	A	B	C	D	E	F	G	H	I	J	K	L	M	N	O
1															
2					Design parameter				Equilibrium		Maximum of y_i-y_{prev} (mm)				
3			Δz_1	$r\Delta_z$	L (m)	D (m)	P_h (kN)	M_h (kN·m)	P_h-Q_0 (kN)	M_h-M_0 (kN·m)					
4			0.4	1.03305343	20	1	160	0	0	7.77×10^{-14}	7.36×10^{-8}				
5															
6		i	z_i (m)	E_pI_p (kN·m²)	y_i (m)	y_i' (m)	k_{secd}	p_i (kN/m)	Q_i (kN)	M_i (kN·m)	y_{prev} (mm)	D (m)	φ (°)	γ (kN/m³)	
7		0	0.000	1262753.12	0.004703	−0.001614	0.0360104	−0.00017	160	-7.77×10^{-14}	4.702646	1.0	35	16.8	
8		1	0.400	1262753.12	0.004058	−0.001604	12705.574	−51.5535	149.68926	62.62523022	4.057095	1.0	35	16.8	
9		2	0.813	1262753.12	0.003399	−0.001574	21613.792	−73.4638	123.85934	119.4550631	3.398538	1.0	35	16.8	
10		3	1.240	1262753.12	0.002736	−0.001526	28733.334	−78.6002	91.402818	165.4785907	2.735177	1.0	35	16.8	
11		4	1.681	1262753.12	0.002075	−0.001463	34928.627	−72.4848	58.089354	198.3417316	2.074964	1.0	35	16.8	
12		5	2.137	303187.024	0.001425	−0.001263	47809.788	−68.1386	26.057741	217.4338331	1.425004	0.7	35	16.8	
13		6	2.607	303187.024	0.000910	−0.000922	54670.271	−49.7494	−1.68272	222.8301537	0.909849	0.7	35	16.8	
14		7	3.093	303187.024	0.000549	−0.000569	60813.744	−33.3681	−21.8878	216.7777407	0.548595	0.7	35	16.8	
15		8	3.596	1262753.12	0.000353	−0.000350	55744.921	−19.6741	−35.2080	202.1517234	0.352859	1.0	35	16.8	
16		9	4.115	1262753.12	0.000193	−0.000271	60450.881	−11.6734	−43.3403	181.5948239	0.193056	1.0	35	16.8	
17		⋮	⋮	⋮	⋮	⋮	⋮	⋮	⋮	⋮	⋮	⋮	⋮	⋮	
18		25	15.18	1262753.12	5.23×10^{-6}	5.00×10^{-7}	132324	−0.69221	1.76349	−2.5025619	5.23×10^{-3}	1.0	35	16.8	
19		26	16.08	1262753.12	4.88×10^{-6}	-8.19×10^{-7}	136985.44	−0.66796	1.150161	−1.1903820	4.88×10^{-3}	1.0	35	16.8	
20		27	17.02	1262753.12	3.70×10^{-6}	-1.40×10^{-6}	141692.41	−0.52485	0.5945195	−0.3880178	3.70×10^{-3}	1.0	35	16.8	
21		28	17.98	1262753.12	2.21×10^{-6}	-1.56×10^{-6}	146447.92	−0.32415	0.1859599	−0.0279268	2.21×10^{-3}	1.0	35	16.8	
22		29	18.97	1262753.12	6.52×10^{-7}	-1.56×10^{-6}	151254.84	−0.09860	−0.0242	0.03390761	6.52×10^{-4}	1.0	35	16.8	
23		30	20.00	1262753.12	-9.33×10^{-7}	-1.54×10^{-6}	156115.96	0.145721	0	0	-9.33×10^{-4}	1.0	35	16.8	
24															

Fig. 2 Spreadsheet method for a laterally loaded pile with a necking defect. The Excel solver is applied to reach the equilibrium; boxed cells contain equations; the yellow highlighted cells are initially set to 0; the blue highlighted cells are the necking section of the cast-in-place pile. The parameters are explained in the text. References to color refer to the online version of this figure

that the length of the laterally loaded pile should be reached at the position of the last node (e.g., z_{30}) (Low et al., 2001). Also, note that i is the node number.

As depicted in Fig. 2, the necking defect is located between Nodes 5 and 7 in Column i. The diameter (in Column D) of the necking defect is 0.7 m. Correspondingly, the bending stiffness of the necking defect in Column E_pI_p is determined as:

$$E_pI_{p1}=E_pI_p\frac{D_1^4}{D^4}, \tag{2}$$

where E_p is the elastic modulus of the pile, I_{p1} is the moment of inertia of the necking defect, which is equal to $\pi D_1^4/64$, and I_p is the moment of inertia of the pile without a necking defect, which is equal to $\pi D^4/64$.

The lateral deflection of the pile is entered into Column y_i (Cells E7–E23), which is defined as:

$$y_i=y_{i+1}+\left(\frac{\Delta z_{i+1}}{\Delta z_{i+2}}\right)^2(y_{i+2}-y_{i+1})-\Delta z_{i+1}\left(1+\frac{\Delta z_{i+1}}{\Delta z_{i+2}}\right)y'_{i+1}, \tag{3}$$

where $\Delta z_{i+1}=z_{i+1}-z_i$ and $\Delta z_{i+2}=z_{i+2}-z_{i+1}$. The final two deflection values, y_{29} and y_{30}, are initially set to zero.

Column y'_i stands for the rotation of the pile at z_i:

$$y'_i=y'_{i+1}-0.5\left[\left(\frac{M}{E_pI_p}\right)_{i+1}+\left(\frac{M}{E_pI_p}\right)_i\right](z_{i+1}-z_i), \tag{4}$$

where M is the bending moment defined later in Eq. (7), and y'_{30} is equal to $(y_{30}-y_{29})/(z_{30}-z_{29})$.

Column k_{secd} stands for the product of the initial stiffness (secant k) and the pile diameter (D). Visual Basic for Applications (VBA) in Microsoft Excel is employed to establish the initial stiffness function. The detailed code is given in Section S1 of the electronic supplementary materials (ESM). The initial stiffness function reads its parameter y from Column y_{prev} in Fig. 2 (starting from Cell K7). A program created by Low et al. (2001) is used to iteratively update the secant k of the p-y curve (note that the p-y curve will be introduced in Section 2.2), in tandem with the updated pile deflections of the Column y_{prev}. This code is provided in Section S2 of the ESM. The reader may also refer to Low et al. (2001) for additional details.

$$p_i=-k_{\sec d}y_i, \tag{5}$$

where p_i is the soil resistance per pile length, and k_{secd} is the product of the initial stiffness (secant k) and the pile diameter (D). The negative sign means that soil resistance acts in the opposite direction to the pile deflection.

The shear force Q and bending moment M are defined as:

$$Q_i=Q_{i+1}-0.5(p_{i+1}+p_i)(z_{i+1}-z_i), \tag{6}$$

$$M_i=M_{i+1}-Q_{i+1}\Delta z_{i+1}+\frac{1}{6}\Delta z_{i+1}^2(2p_{i+1}+p_i). \tag{7}$$

The shear force and bending moment at the pile toe (Q_{30} and M_{30}) are set to zero (in Cells I23 and J23, respectively). To be in equilibrium, the computed values of Q_0 and M_0 at z_0 must be equivalent to the applied horizontal force (P_h) and moment (M_h), respectively. The equilibrium conditions, which are shown in Cells I3 and J3 of Fig. 2, are defined as:

$$Q_0-P_h=0, \tag{8}$$

$$M_0-M_h=0. \tag{9}$$

These two equations have been entered in Fig. 2 under the heading "Equilibrium". Note that Q_0 and M_0 in Eqs. (8) and (9) can only be determined through recursive numerical calculation by satisfying the relationships among y_i, y_i', p_i, Q_i, and M_i (at all nodal points i), according to Eqs. (3)–(7).

2.2 *p-y* curve

The p-y curve for sand recommended by the American Petroleum Institute (API, 2011) is adopted in the spreadsheet method to simulate the interaction between the pile and the sand:

$$p=Ap_u\tanh\left(\frac{kz}{Ap_u}y\right), \tag{10}$$

where A is the depth correction coefficient, which is equal to $3.0-0.8(z/D)\geqslant 0.9$ (Reese et al., 1974). k is the initial foundation reaction modulus, which is $(0.008085\times\varphi^{2.45}-26.09)\times10^3$ (Augustesen et al., 2009). φ is the friction angle of the sand. y is the deflection of the pile at a depth z, and p_u is the ultimate soil reaction, which is determined as (API, 2011):

$$p_u=\min\{(C_1z+C_2D)\sigma'_v,\ C_3D\sigma'_v\}, \tag{11a}$$

$$\sigma'_v=\gamma z, \tag{11b}$$

where σ'_v is the effective overburden pressure at a given depth z, γ is the unit weight of the sand, and C_1, C_2, and C_3 are the ultimate soil reaction coefficients, which are determined as (Augustesen et al., 2009):

$$C_1=0.115\times10^{0.0405\varphi}, \tag{12a}$$
$$C_2=0.571\times10^{0.0220\varphi}, \tag{12b}$$
$$C_3=0.646\times10^{0.0555\varphi}. \tag{12c}$$

These equations are embedded in the spreadsheet method using the VBA program, which can then be used to update the initial stiffnesses in Column k_{secd}. In this study, the initial stiffness of the *p*-*y* curve for sand proposed by Kallehave et al. (2012) is adopted:

$$K=k_{API}z_{ref}\left(\frac{z}{z_{ref}}\right)^{0.6}\left(\frac{D_{ref}}{D}\right)^{0.5}, \tag{13}$$

where K is the initial stiffness of the *p*-*y* curve for sand, k_{API} is the initial stiffness modulus, and z_{ref} and D_{ref} are equal to 2.50 m and 0.61 m, respectively.

2.3 Calculation procedure

To start the calculation, the lateral deflections at the last two nodes of the pile are initially set to zero, first rendering the pile straight along its entire length. Microsoft Excel and its built-in optimization routine, Solver, are used to calculate the pile deflection as follows: "set" Eq. (8) equal to zero, "by changing" (automatically) the values of the lateral defections y at the bottom two nodes, "subject to" the constraint that Eq. (9) equals zero. The Solver option "Use automatic scaling" is also selected. Other Solver options (precision, estimates, derivatives, and search method) are left at their default settings. The program "Sub Iterate_ksecd" (Section S2 of the ESM) is then executed to invoke the Solver repeatedly using the preset scenario. Each time the program "Iterate_ksecd" (Section S1 of the ESM) modifies the "y_{prev}" column in its For/Next loop, the values in the "k_{secd}" column shown in Fig. 2 are updated automatically.

2.4 Robust geotechnical design

According to the framework of RGD, the input parameters used in the spreadsheet method can be divided into two categories: noise factors and design parameters. The position, diameter, and length of a necking defect, together with the friction angle and unit weight of the sand, are regarded as noise factors that exhibit considerable uncertainty. These noise factors could be estimated using statistical data from on-site investigations and/or geotechnical tests. However, obtaining in-situ data is time-consuming and expensive, which is why some sites have limited data on soil parameters for design applications. Because of such cases, researchers such as Kharmanda and Antypas (2016), Phoon et al. (2022), and Li et al. (2023) have established databases for soil parameters and provided guidance on evaluating uncertainties in these parameters. Thus, the statistical parameters (e.g., the type of distribution, mean value, and coefficient of variation) can be determined using the aforementioned methods.

The length (L) and diameter (D) of the pile are regarded as the design parameters that can be set by the designers. Based on the chosen design parameters, the cost of a certain design can be estimated. In practical engineering, the cost function is typically determined based on local experience and industry requirements. For the sake of simplicity, we consider the volume of the laterally loaded pile to be the cost (C):

$$C=\frac{\pi D^2 L}{4}. \tag{14}$$

For each set of design parameters, the spreadsheet method (presented in Section 2.1) is used to establish the calculation model of the pile. In the calculation model, MCS is applied to generate N sets of noise factors. Subsequently, N sets of the deflection, bending moment, and shear force of the laterally loaded pile are obtained, from which mean values and standard deviations can be determined. In this study, we use the standard deviation of the pile deflection at the ground surface to assess the design robustness. A minor variation in the deflection of the pile at the ground surface (in terms of standard deviation) indicates enhanced design robustness. The objective of the RGD is to render the standard deviation of the deflection of the pile insensitive to variations in the noise factors (e.g., the diameter and length of necking defects, the friction angle, and the unit weight of sand) by adjusting the design parameters. At the same time, safety requirements for the laterally loaded pile must be satisfied.

Two safety requirements are considered in this work. One is the factor of safety (FOS, F_s), which is defined as the ratio of the maximum bending moment and the ultimate bending moment of the pile:

$$F_S = \frac{M_u}{\bar{M}_{max}}, \tag{15}$$

where $\bar{M}_{max}$ is the mean value of the N sets of maximum bending moments as calculated by the spreadsheet method. M_u is the ultimate bending moment of the pile, which can be determined as (MOHURD, 2011):

$$M_u = \frac{2}{3} \times \alpha_1 f_c r S \frac{\sin^3(\pi\alpha)}{\pi}, \tag{16}$$

where f_c is the compressive strength of the concrete. α_1 is equal to 1 when the concrete strength grade is lower than C50. r and S are the radius and area of a pile with a circular cross-section, respectively. α is the central angle (in radians) of the compressive zone of the circular cross-section, which is equal to 1/3. In this paper, the target FOS of the pile is larger than 1.5.

The other safety requirement is that the mean value of pile deflection at the ground surface should be less than a standard value. In accordance with the technical code for building pile foundations (MOC, 2008), a permissible pile deflection is less than 6–10 mm. In this work, we set the allowable pile deflection at the ground surface to 6 mm.

Designs that satisfy these two safety requirements are considered as feasible designs in the RGD. Given the inherent conflict between cost and design robustness for the feasible designs, the Pareto front and knee point are utilized to identify the optimal design out of the various candidates. As a result, the optimal design derived from the proposed framework can simultaneously consider the safety, design robustness, and cost of the laterally loaded pile. For further insights into the Pareto front and knee point, please refer to Section S3 of the ESM.

3 Design framework

A flowchart for the robust design workflow for a laterally loaded pile considering necking defects is shown in Fig. 3, and its main steps can be summarized as follows:

Step 1: Define the problem, and then categorize all input parameters into design parameters and noise factors.

Step 2: Determine the design space and characterize the uncertainties in the noise factors. The design parameters, which should be selected based on local experience and their typical ranges, are specified in discrete numbers. The total number of possible designs in the design space is represented by M_{ds}. Uncertainties in noise factors are usually quantified based on data from field surveys and supplemented by local experience. N sets of noise factors are generated by the MCS.

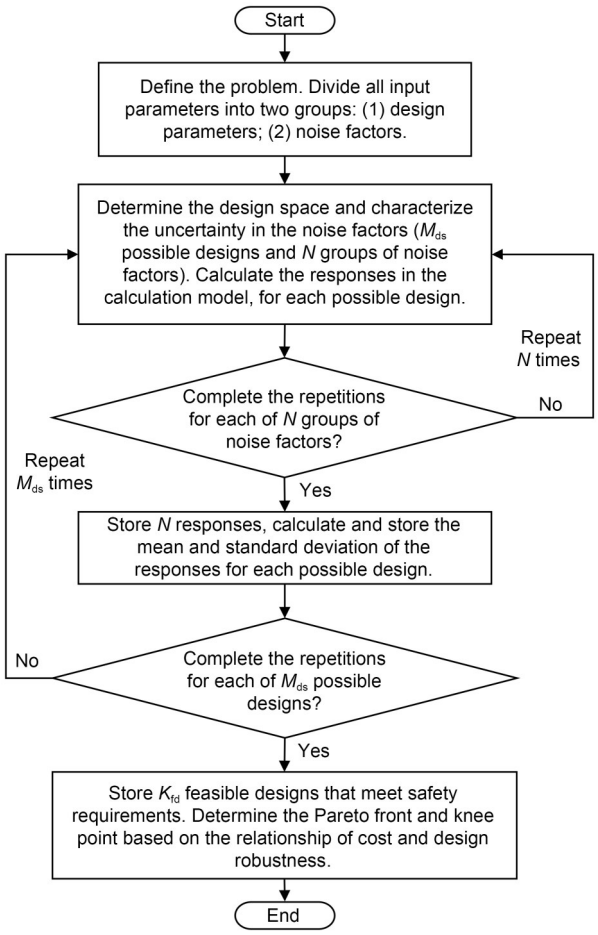

Fig. 3 Flowchart for the robust design of a laterally loaded pile considering necking defects

Step 3: For each set of possible design parameters, the responses (deformation, bending moment, and shear force) of the laterally loaded pile are calculated according to N sets of noise factors. The mean value of the N sets of the maximum bending moments is used to evaluate the safety requirements. The standard deviation of the lateral pile deflection at the ground surface is used to measure the robustness of a feasible design that fulfills the safety requirements. The cost of the feasible design is estimated using Eq. (14). Then, a number (K_{fd}) of feasible designs are obtained.

Step 4: Obtain the Pareto front and knee point based on the relationship between cost and design robustness. The knee point is the most preferred design, as it can balance design robustness and cost. The reader can refer to Section S3 of the ESM for more details about establishing the Pareto front and knee point.

4 Validation and application

4.1 Validation with experimental data

In this study, the spreadsheet method is validated using experimental data from Hariswaran and Premalatha (2021). A schematic of the experimental setup in the research of Hariswaran and Premalatha (2021) is shown in Fig. 4. A solid aluminum pipe with a diameter (D) of 20 mm is adopted as the model pile, consistent with the conceptual pile depicted in Fig. 1. The bending stiffness of the model pile is 542.0×10^6 N·mm^2. Three length-to-diameter ratios (L/D) of the model pile, which are 20, 30, and 40, are used in the experiments. The diameter and length of the necking defect are D_1= 16 mm and l=80 mm, respectively. The necking defect is positioned at depths below the ground surface (L_1) ranging from 40 to 320 mm, in 40 mm increments. The load–deflection curve for the L/D=20 model pile is measured, along with the ultimate lateral loads for L/D=30 and 40 piles.

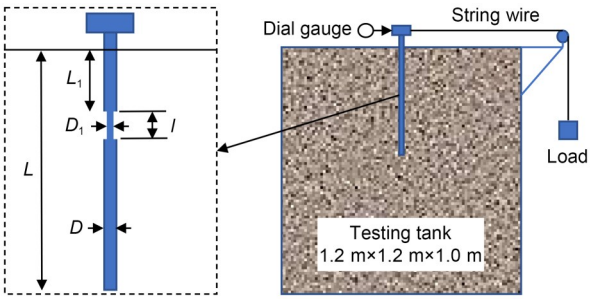

Fig. 4 Schematic of the experimental setup for the laterally loaded pile with necking defects (modified from Hariswaran and Premalatha (2021))

The model piles are embedded in sand within a 1.2 m×1.2 m×1.0 m testing tank. Silt with mass fraction of 2% is contained in the sand. The maximum and minimum dry densities of the sand are 1806 and 1543 kg/m^3, respectively. Direct shear tests indicate friction angles of 31°, 35°, and 40° for sand with relative densities of 30%, 50%, and 70%, respectively. The unit weight of the sand is derived from its relative density using the following relationship:

$$R_D=\frac{\rho_d-\rho_{d\min}}{\rho_{d\max}-\rho_{d\min}}\times\frac{\rho_{d\max}}{\rho_d}, \tag{17a}$$

$$\gamma=\rho_d\times g, \tag{17b}$$

where R_D is the relative density, ρ_d is the dry density, ρ_{dmax} is the maximum dry density, ρ_{dmin} is the minimum dry density, and g is the acceleration due to gravity (which is set to 9.81 m/s^2). Using Eqs. (17a) and (17b), the maximum, minimum, and average unit weight of the sand are determined as 18.0, 15.4, and 16.6 kN/m^3, respectively.

A monotonically-increasing lateral load is applied on the top of the pile by a string wire until the lateral deflection of the pile at the ground surface reaches 4 mm, at which point the ultimate lateral bearing capacity of the pile is achieved. The loading process in these experiments is simulated by the spreadsheet method described in Section 2. The load–deflection curves are obtained and then compared with the experimental measurements. Fig. 5 presents a comparison

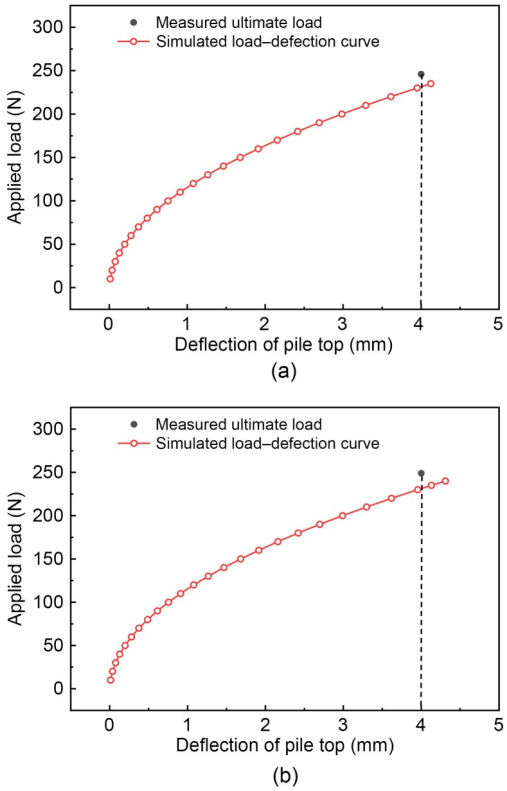

Fig. 5 Comparison between the simulated and measured ultimate loads for piles with (a) L/D=30 and (b) L/D=40

between the simulated and the measured ultimate bearing capacities of the pile without a necking defect. For sand with a relative density of 50%, when the lateral deflection at the ground surface reaches 4 mm, the simulated and measured loads at the pile head are 232 and 246 N (L/D=30), respectively. For L/D=40, the corresponding values are 233 N (simulated) and 249 N (measured). Thus, strong agreement is observed between the simulated and measured ultimate loads.

Fig. 6 shows a comparison between the simulated and measured load–deflection curves for piles with an L/D ratio of 20. The model pile has a total length (L) of 400 mm. The necking defects are positioned at depths of 80 mm (0.2L), 160 mm (0.4L), 240 mm (0.6L), and 320 mm (0.8L) below the ground surface. The results demonstrate that the simulated curves accurately capture the nonlinear behavior observed in the experimental load–deflection data. The simulated loads closely match the measured values across all lateral deflection levels at the ground surface. As the necking defect is placed deeper (from 80 to 320 mm below the surface), the ultimate load increases; this trend is accurately predicted by the proposed spreadsheet method.

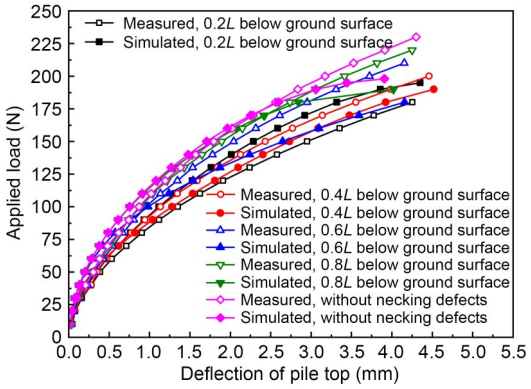

Fig. 6 Comparison between the simulated and measured load–deflection curves of the piles with necking defects at various depths

4.2 Application of the proposed method

The prototype pile corresponding to the model pile used by Hariswaran and Premalatha (2021) is next taken as an example to illustrate the proposed method and framework. Hariswaran and Premalatha (2021) reported that the prototype pile is a reinforced concrete pile with a diameter of 1000 mm. The scaling factor (n) between the prototype pile and model pile is calculated using Eq. (18) and yields n=26 (Hariswaran and Premalatha, 2021):

$$E_{\mathrm{p}}I_{\mathrm{p}}=E_{\mathrm{m}}I_{\mathrm{m}}n^{4.5}, \tag{18}$$

where $E_{\mathrm{p}}I_{\mathrm{p}}$ and $E_{\mathrm{m}}I_{\mathrm{m}}$ are the bending stiffness of the prototype pile and the bending stiffness of the model pile, respectively.

Based on Eq. (18) and the scaling factor, the bending stiffness of the prototype pile can be determined as 126.3×10^4 kN·m^2. Because the L/D values of the model piles are 20, 30, and 40, and D is equal to 1000 mm, the lengths of the prototype piles L are equal to 20, 30, and 40 m. The diameter of the necking defect of the prototype pile ranges from 0.7D to 0.9D. The length of the necking defect of the prototype pile ranges from 0.1L to 0.4L. The friction angle of the sand is between 30° and 40°. The unit weight of sand is between 15 and 18 kN/m^3. The prototype pile is subjected to a lateral load of 200 kN. These parameters used for the model and prototype piles are summarized in Table 1.

Recall that the parameters can be categorized into design parameters and noise factors in the framework of RGD. Design parameters are specified by the engineer during the optimization process. For the prototype pile, the design parameters are the length and diameter of the pile. The length of the pile (L) ranges from 20 to 40 m, in increments of 2 m. The diameter of the pile (D) ranges from 0.6 to 1.4 m, in increments

Table 1 Parameters of the model and prototype piles

Parameter	Description	
	Model pile (solid aluminum pile)	Prototype pile (reinforced concrete pile)
Bending stiffness	542.0×10^6 N·mm^2	126.3×10^4 kN·m^2
Diameter of the pile	20 mm	1000 mm
Length of the pile	400, 600, and 800 mm	[20 m, 40 m]
Diameter of the necking defect	14, 16, and 19 mm	[0.7D, 0.9D]
Length of the necking defect	[0.1L, 0.4L]	[0.1L, 0.4L]
Friction angle	31°, 35°, 40°	[30°, 40°]
Unit weight	15–18 kN/m^3	15–18 kN/m^3

of 0.2 m. This results in 55 candidate designs within the design space, each representing a unique combination of discrete L and D values.

The position, diameter, and length of the necking defect, as well as the friction angle and unit weight of the sand, are considered as noise factors. Their uncertainties should thus be quantified. Due to the lack of in-situ data for the noise factors, the position of the necking defect is assumed to be uniformly distributed between 0.1L and 0.8L depth below the sand surface. The diameter of the necking defect is taken to be uniformly distributed between 0.7D and 0.9D. The length of the necking defect is assumed to be uniformly distributed between 0.1L and 0.4L. The friction angle of the sand is assumed to exhibit a uniform distribution between 30° and 40°. The unit weight of the sand is assumed to be uniformly distributed between 15 and 18 kN/m^3.

4.3 Optimal result

Next, the noise factors are randomly generated by the MCS. However, the ideal number of realizations is an important parameter that must be determined. The coefficient of variation (COV) of pile deflection at the ground surface with varying MCS realization numbers is calculated using the spreadsheet method from Section 2. The results are presented in Fig. 7. When the number of MCS realizations exceeds 150, the COV of deflection at the ground surface exhibits asymptotic convergence toward stability. To balance computational efficiency and accuracy, the number of MCS realizations is taken as 200, aligning with the sensitivity analysis shown in Fig. 7.

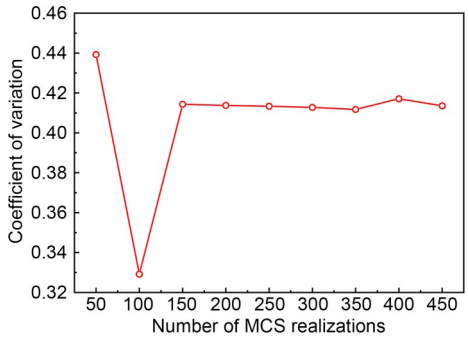

Fig. 7 COVs of the pile deflection at the ground surface corresponding to different MCS realization numbers

For illustrative purposes, the design robustness and cost of all 55 designs within the design space are calculated and presented in Fig. 8. The hollow circles indicate designs that fail to meet the safety requirements; the solid red circles represent the feasible designs that satisfy the safety requirements. A total of 29 feasible designs are obtained out of the 55 designs in the space. In accordance with the procedures detailed in Section S3 of the ESM, the Pareto front and knee point can be determined using the feasible designs.

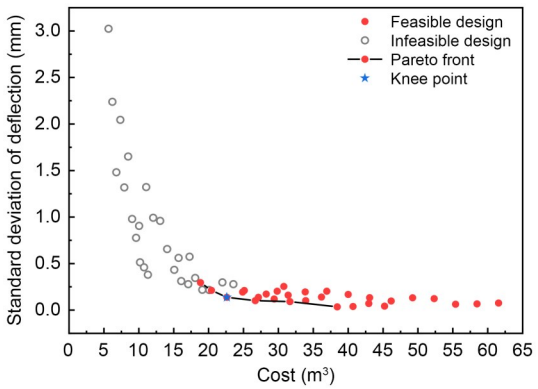

Fig. 8 Design robustness and cost of all 55 designs within the design space. References to color refer to the online version of this figure

The design parameters for the designs on the Pareto front illustrated in Fig. 8 are presented in Table S1 in the ESM. As demonstrated by Khoshnevisan et al. (2014), the knee point of the Pareto front can be identified through the minimum distance method, which is outlined in Section S3 of the ESM. In our investigation, the optimal design parameters corresponding to the knee point are determined as L=20 m and D=1.2 m.

The design corresponding to the knee point (L=20 m and D=1.2 m) could be the optimal design if there is no preference for budget or design robustness. In practice, the designer could select an optimal design from the designs on the Pareto front according to their specific budgeting needs or target design robustness. Taking Table S1 in the ESM as an example, if the highest allowable cost for a project is 30 m^3, the design parameters corresponding to Designs 1 to 4 could be selected as the optimal designs since their costs are under 30 m^3. The optimal design could also be determined according to other factors, such as convenience and time-efficiency of the installation, which are not considered in our design framework. If there is a preference for the design robustness (a target standard deviation of deflection) for the sake of infrastructure

deformation control, the optimal design could be selected out of the designs on the Pareto front according to the target standard deviation of deflection.

5 Discussion on optimization factors

5.1 Position of the necking defects

The experimental results presented by Hariswaran and Premalatha (2021) indicate that a deeper positioned necking defect has a minimal impact on the lateral deflection and bearing capacity of a pile. This finding may also influence the obtained final optimal designs. To elucidate this point, consider that the position of the necking defect is fixed at depths of 0.1L–0.2L, 0.2L–0.3L, 0.3L–0.4L, 0.4L–0.5L, and 0.5L–0.6L, respectively. The diameter and length of the necking defect are the same as in the previous example. The Pareto fronts corresponding to different positions are shown in Fig. 9. We can see that the design robustness is the lowest when the necking defect is located in the depths of 0.1L–0.2L. As the defect becomes more deeply buried, the design robustness improves. When the position is deeper than 0.4L, the standard deviation of the pile deflection at the ground surface is zero. This indicates that the positioning of the necking defect has no impact on the optimal designs. This finding is consistent with the results reported by Xu and Guo (2021), who experimentally investigated the influence of necking defects on the vertical bearing capacity of piles.

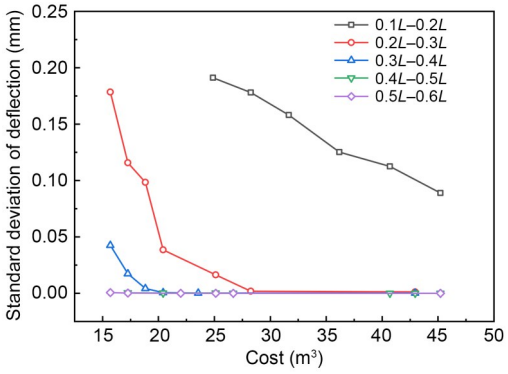

Fig. 9 Pareto fronts for necking defects located at different depths

To investigate why deeper necking defects minimally influence the optimal results, deflections, shear forces, and bending moments of laterally loaded piles with necking defects are calculated and plotted in Fig. 10, using depths of 0.1L–0.2L (black), 0.2L–0.3L (red), 0.3L–0.4L (green), and 0.4L–0.5L (blue). The pile dimensions are set to L=22 m and D=1.0 m for this analysis. For each defect position (e.g., 0.1L–0.2L), the noise factors are identical to those defined in Section 4.2. An MCS with 300 realizations is executed, thus generating 300 sets of deflections, shear forces, and bending moments per defect position. Fig. 10 reveals that these responses are primarily distributed in depths of 0–0.4L. Specifically, Fig. 10c indicates that the maximum bending moment occurs at 0.1L–0.2L (2.2–4.4 m), followed by decreasing magnitudes in the 0.2L–0.3L and 0.3L–0.4L ranges. In addition, below 0.4L, the bending moments are negligible.

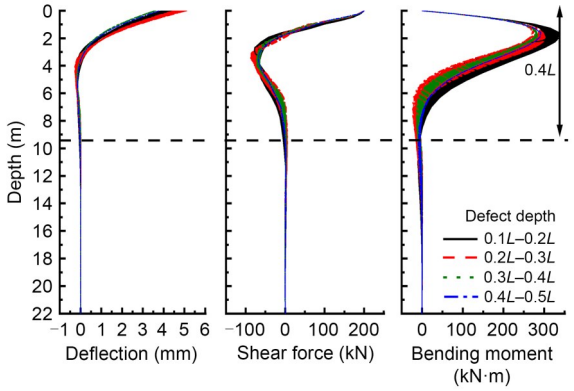

Fig. 10 Deflections, shear forces, and bending moments with necking defects located at different depths (L=22 m, D=1.0 m, and each color is composed of 300 lines). References to color refer to the online version of this figure

If necking defects occur in regions with significant bending moments (e.g., 0.1L–0.2L or 0.2L–0.3L), the reduced bending stiffness amplifies deflection variability (i.e., poor design robustness, as shown in Fig. 9) due to noise factor variations (black and red lines in Fig. 10a). Conversely, defects in deeper regions (e.g., 0.3L–0.4L or beyond 0.4L) induce smaller bending moments, leading to lower deflection variability (improved robustness) under noise variations (green and blue lines in Fig. 10a). Therefore, the influence of necking defect position on the optimal results (Fig. 9) is predominantly governed by the bending moment distribution in laterally loaded piles.

5.2 Friction angle of sand

To investigate the influence of sand friction angle on the optimal results, the responses of laterally loaded

piles are calculated under two conditions: the friction angles of the sand varying in 24°–46°, and varying in 28°–42°; the other parameters are consistent with those used in Section 4.2. Fig. 11 shows the feasible and infeasible designs for both friction angle cases. When the friction angle varies in 24°–46°, the standard deviations of deflection for infeasible designs are slightly larger than those under the 28°–42° condition. This occurs because infeasible designs (with smaller pile lengths and diameters) have lower costs, making them more sensitive to variations in friction angle. In contrast, feasible designs exhibit minimal sensitivity.

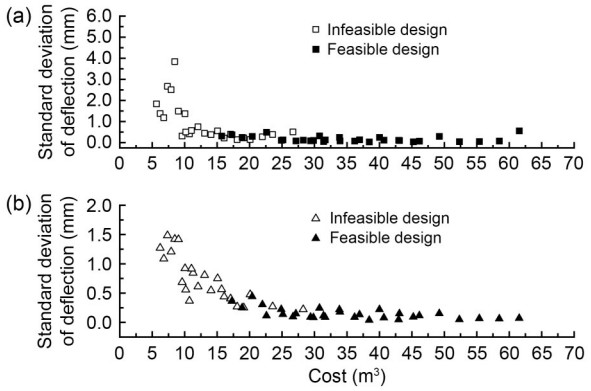

Fig. 11 Infeasible and feasible designs for friction angles varying between 24° and 46° (a) and between 28° and 42° (b)

To clarify this relationship, Fig. 12 presents the Pareto fronts for both friction angle ranges alongside the reference case from Fig. 8. The negligible differences between these three Pareto fronts indicate that sand friction angle variation has a limited impact on the optimal designs in this study. Feasible designs inherently employ larger parameters (selected to meet the safety requirements in Section 2.4), which are less sensitive to the friction angle. Thus, incorporating safety requirements (e.g., the FOS for laterally loaded piles) into the RGD framework not only improves structural safety but also promotes designs with greater robustness (lower deflection variability).

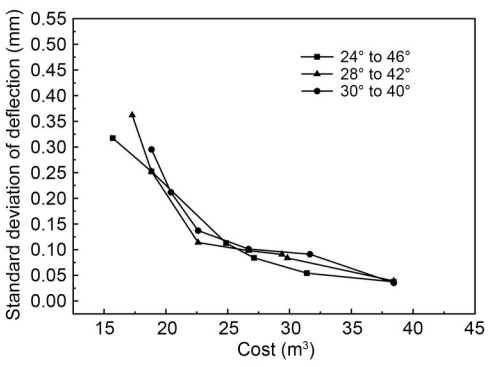

Fig. 12 Pareto fronts corresponding to variations in the friction angle of sand

6 Conclusions

A spreadsheet method was developed and validated for evaluating the mechanical responses of a laterally loaded foundation pile with necking defects. By leveraging the concept of RGD, the framework was aimed at mitigating the effects of necking defects. The efficacy of the method was substantiated through validation with experimental data.

The spreadsheet method was shown to be an effective tool for evaluating the responses of laterally loaded piles with necking defects. A comparison of the proposed method with experimental data demonstrated that it is both accurate and efficient, thereby providing a robust design procedure.

Because of the inherent uncertainties associated with soil parameters and the potential for necking defects, the RGD methodology was effectively applied to mitigate the impact of such defects on laterally loaded piles. Accordingly, the framework comprehensively balances the cost, design robustness, and safety of the pile. The proposed design method may therefore be an effective way to address necking defects during the design stage.

We found that when the necking defect is situated deeper within the pile structure, the overall robustness of the design is enhanced. When the position of the necking defect is deeper than $0.4L$, the influence of the necking defect on the design robustness is minimal due to the distribution characteristics of bending moments along the pile.

Large variations in the friction angle of sand were found to significantly influence the standard deviation of deflection for piles with infeasible design parameters (which are smaller than those of feasible designs). These variations have little influence on the optimal designs since they employ larger design parameters, which are selected based on safety requirements, and are thus insensitive to such variations.

Although the proposed method is time-efficient and well-suited for reliability analysis in the case of

this study, its effectiveness and accuracy for more complicated geological conditions warrant further investigation. The interaction between the soil and pile would be more complicated in such conditions, so a series of nonlinear springs (*p-y* curve) may not accurately capture the nonlinear behavior of the soil and the pile in the 3D space. Therefore, a high efficiency method with accurate reliability-based design in complex environments would need to be developed in future research.

Acknowledgments

This work is supported by the Fundamental Research Funds for the Central Universities of China (No. 226-2024-00197), the National Natural Science Foundation of China (No. 42277129), the Key R&D Project of Zhejiang Province (No. 2021C03159), and the Natural Science Foundation of Zhejiang Province (No. LR24E080004), China.

Author contributions

Yang YU and Qing LÜ designed the research. Yang YU and Bo SHI developed the method and wrote the first draft of the manuscript. Chaofeng WU helped to organize the manuscript. Yang YU revised and edited the final version.

Conflict of interest

Yang YU, Bo SHI, Qing LÜ, and Chaofeng WU declare that they have no known competing financial interests or personal relationships that could have appeared to influence the work reported in this paper.

References

API (American Petroleum Institute), 2011. Geotechnical and Foundation Design Considerations, ANSI/API RP 2GEO: 2011. API, Washington, USA.

Augustesen AH, Brødbæk KT, Møller M, et al., 2009. Numerical modelling of large-diameter steel piles at Horns Rev. Proceedings of the 12th International Conference on Civil, Structural and Environmental Engineering Computing, article 239.
https://doi.org/10.4203/ccp.91.239

Fattah MY, Al-Shakarchi Y, Kadhim YM, 2010. Investigation on the use of micropiles for substitution of defected piles by the finite element method. *Journal of Engineering*, 16(3): 5300-5314.
https://doi.org/10.31026/j.eng.2010.03.02

Hariswaran S, Premalatha K, 2021. Experimental investigation on the behavior of a defective pile subject to a lateral load. *Soil Mechanics and Foundation Engineering*, 58(4): 339-346.
https://doi.org/10.1007/s11204-021-09747-7

Juang CH, Wang L, 2013. Reliability-based robust geotechnical design of spread foundations using multi-objective genetic algorithm. *Computers and Geotechnics*, 48:96-106.
https://doi.org/10.1016/j.compgeo.2012.10.003

Kallehave D, Thilsted CL, Liingaard MA, 2012. Modification of the API *p-y* formulation of initial stiffness of sand. Proceedings of the Offshore Site Investigation and Geotechnics: Integrated Technologies–Present and Future, p.465-472.

Kharmanda GM, Antypas IR, 2016. Reliability-based design optimization strategy for soil tillage equipment considering soil parameter uncertainty. *Advanced Engineering Research*, 16(2):136-147.
https://doi.org/10.12737/19690

Khoshnevisan S, Gong WP, Wang L, et al., 2014. Robust design in geotechnical engineering-an update. *Georisk: Assessment and Management of Risk for Engineered Systems and Geohazards*, 8(4):217-234.
https://doi.org/10.1080/17499518.2014.980274

Khoshnevisan S, Wang L, Juang CH, 2017. Response surface-based robust geotechnical design of supported excavation-spreadsheet-based solution. *Georisk: Assessment and Management of Risk for Engineered Systems and Geohazards*, 11(1):90-102.
https://doi.org/10.1080/17499518.2016.1247285

Lee JS, Song JU, Hong WT, et al., 2018. Application of time domain reflectometer for detecting necking defects in bored piles. *NDT & E International*, 100:132-141.
https://doi.org/10.1016/j.ndteint.2018.09.006

Li HJ, Tong LY, Liu SY, et al., 2018. Construction and verification of a unified *p-y* curve for laterally loaded piles. *Bulletin of Engineering Geology and the Environment*, 77(3):987-997.
https://doi.org/10.1007/s10064-017-1111-7

Li JP, Zhang J, Liu SN, et al., 2015. Reliability-based code revision for design of pile foundations: practice in Shanghai, China. *Soils and Foundations*, 55(3):637-649.
https://doi.org/10.1016/j.sandf.2015.04.014

Li KQ, Yin ZY, Liu Y, 2023. Influences of spatial variability of hydrothermal properties on the freezing process in artificial ground freezing technique. *Computers and Geotechnics*, 159:105448.
https://doi.org/10.1016/j.compgeo.2023.105448

Low BK, Teh CI, Tang WH, 2001. Stochastic nonlinear *p-y* analysis of laterally loaded piles. Proceedings of the International Conference on Structural Safety and Reliability.

MOC (Ministry of Construction of the People's Republic of China), 2008. Technical Code for Building Pile Foundations, JGJ 94-2008. National Standards of the People's Republic of China (in Chinese).

MOHURD (Ministry of Housing and Urban-Rural Development of the People's Republic of China), 2011. Code for Design of Concrete Structures, GB/T 50010-2010. National Standards of the People's Republic of China (in Chinese).

Peng X, Li DQ, Cao ZJ, et al., 2017. Reliability-based robust geotechnical design using Monte Carlo simulation. *Bulletin of Engineering Geology and the Environment*, 76(3): 1217-1227.
https://doi.org/10.1007/s10064-016-0905-3

Phoon KK, Cao ZJ, Ji J, et al., 2022. Geotechnical uncertainty,

modeling, and decision making. *Soils and Foundations*, 62(5):101189.
https://doi.org/10.1016/j.sandf.2022.101189

Poulos HG, 2005. Pile behavior—consequences of geological and construction imperfections. *Journal of Geotechnical and Geoenvironmental Engineering*, 131(5):538-563.
https://doi.org/10.1061/(asce)1090-0241(2005)131:5(538)

Reese LC, Cox WR, Koop FD, 1974. Analysis of laterally loaded piles in sand. Proceedings of the Offshore Technology Conference.
https://doi.org/10.4043/2080-ms

Schmoor KA, Achmus M, 2020. Reliability-based evaluation of offshore design approaches for tensile piles in noncohesive soil. *International Journal of Offshore and Polar Engineering*, 30(2):240-247.
https://doi.org/10.17736/ijope.2020.cl15

Stuedlein AW, Neely WJ, Gurtowski TM, 2012. Reliability-based design of augered cast-in-place piles in granular soils. *Journal of Geotechnical and Geoenvironmental Engineering*, 138(6):709-717.
https://doi.org/10.1061/(asce)gt.1943-5606.0000635

Sun YZ, Sun HL, Tang C, et al., 2023. Monotonic uplift behavior of anchored pier foundations in soil overlying rock. *Journal of Zhejiang University-SCIENCE A*, 24(7):569-583.
https://doi.org/10.1631/jzus.A2200446

Wang Z, Yu Y, Sun HY, et al., 2020. Robust optimization of the constructional time delay in the design of double-row stabilizing piles. *Bulletin of Engineering Geology and the Environment*, 79(1):53-67.
https://doi.org/10.1007/s10064-019-01554-7

Xu KJ, Poulos HG, 2000. Measured and predicted axial response of piles with diameter discontinuities. *Geotechnical Engineering*, 31(3):171-191.

Xu ZJ, Guo ZX, 2021. Experimental study on bearing characteristics and soil deformation of necking pile with cap using transparent soils technology. *Advances in Civil Engineering*, 2021:6625556.
https://doi.org/10.1155/2021/6625556

Yu Y, Li XM, Pan XH, et al., 2020. A robust and efficient method of designing piles for landslide stabilization. *Environmental & Engineering Geoscience*, 26(4):481-492.
https://doi.org/10.2113/EEG-2333

Yu YS, Li LL, Kong XM, et al., 2024. Deformation and stability of the seawall, considering the strength uncertainty of cement mixing piles. *Journal of Zhejiang University-SCIENCE A*, 25(6):483-501.
https://doi.org/10.1631/jzus.A2300180

Zhou P, Xu JH, Xu CJ, et al., 2024. Influence of the penetration of adjacent X-section cast-in-place concrete (XCC) pile on the existing XCC pile in sand. *Journal of Zhejiang University-SCIENCE A*, 25(7):557-572.
https://doi.org/10.1631/jzus.A2300384

Electronic supplementary materials

Sections S1–S3, Table S1